Computer Science Department of The University of Auckland
CITR at Tamaki Campus (http://www.citr.auckland.ac.nz/)

CITR-TR-123 Jan 2003

A Review on Research and Applications of Cylindrical Panoramas

Reinhard Klette, Georgy Gimelfarb [1], Shou KangWei [2], Fay Huang [3], Karsten Scheibe, Martin Scheele, Anko Börner [4], and Ralf Reulke [5]

Abstract

This paper reviews research related to the design, production and application of cylindrical panoramic cameras. Such a camera is characterized by rotating linear sensors capturing one image column at a time. This allows for accurate mappings onto a cylindrical image surface and very high image resolutions paid by motion distortions in dynamic scenes. These panoramic images can be used, for example, for stereo visualization and stereo reconstruction in applications where extremely high image resolution is of benefit (for static scenes). The paper deals especially with aspects of stereo visualization and reconstruction.

1 r.klette@auckland.ac.nz, g.gimelfarb@auckland.ac.nz
CITR, The University of Auckland, Auckland, New Zealand

2 shoukang@ozawa.ics.keio.ac.jp
Dep. of Information and Computer Science, Keio University, Yokohama, Japan

3 fayhuang@iis.sinica.edu.tw
Inst. of Information Science, Academia Sinica, Nankang, Taipei, Taiwan

4 Karsten.Scheibe@dlr.de, Martin.Scheele@dlr.de, Anko.Boerner@dlr.de
Inst. of Space Sensor Technology and Planetary Exploration, DLR, Berlin, Germany

5 Ralf.Reulke@ifp.uni-stuttgart.de
Institute for Photogrammetry, Stuttgart University, Stuttgart, Germany

A Review on Research and Applications of Cylindrical Panoramas

Reinhard Klette, Georgy Gimelfarb *
CITR, The University of Auckland, Auckland, New Zealand
Shou Kang Wei †
Dep. of Information and Computer Science, Keio University, Yokohama, Japan
Fay Huang ‡
Inst. of Information Science, Academia Sinica, Nankang, Taipei, Taiwan
Karsten Scheibe, Martin Scheele, Anko Börner §
Inst. of Space Sensor Technology and Planetary Exploration, DLR, Berlin, Germany
Ralf Reulke ¶
Institute for Photogrammetry, Stuttgart University, Stuttgart, Germany

Abstract

This paper reviews research related to the design, production and application of cylindrical panoramic cameras. Such a camera is characterized by rotating linear sensors capturing one image column at a time. This allows for accurate mappings onto a cylindrical image surface and very high image resolutions paid by motion distortions in dynamic scenes. These panoramic images can be used, for example, for stereo visualization and stereo reconstruction in applications where extremely high image resolution is of benefit (for static scenes). The paper deals especially with aspects of stereo visualization and reconstruction.

Keywords:

1 Introduction

A single-line line camera is geometrically characterized by a single optical (projection) center, denoted as **C**, and a 1D linear photon-sensing device (e.g. CCD). Let f denote the camera's focal length. To acquire a cylindrical panoramic image, a slit camera rotates with respect to a fixed 3D axis (e.g. the rotation axis of a turntable) and captures slit images consecutively at equidistant angles γ. Each slit image contributes to a single column of the resulting panoramic image. The camera setup of the panorama acquisition is shown in Fig. 1. The off-axis distance R, principal angle ω and the camera focal length f remain constant during a panoramic image acquisition process. Let $E_{\mathcal{P}}$ denote a panoramic image. We write $E_{\mathcal{P}}(R, f, \omega, \gamma)$ to specify the camera parameters of a panoramic image.

Several results in this review are citations from [Huang 2002; Wei 2002].

Recent studies of these types of camera models [Klette et al. 2001] are in close relation to developments in camera design: Fig. 1 (left) shows a single-line panorama camera (built at DLR) which may rotate part of, or full $360°$. This color camera produces line images having 10,200 pixels each, and a full $360°$ image has 55,000 columns for f = 60 mm which results in a single panoramic image of size 3.3 gigabytes. The radiometric dynamics is 14 bits and the signal to noise ratio is in the range of 8 bits. The acquisition time depends from the illumination conditions and is about 4 minutes.

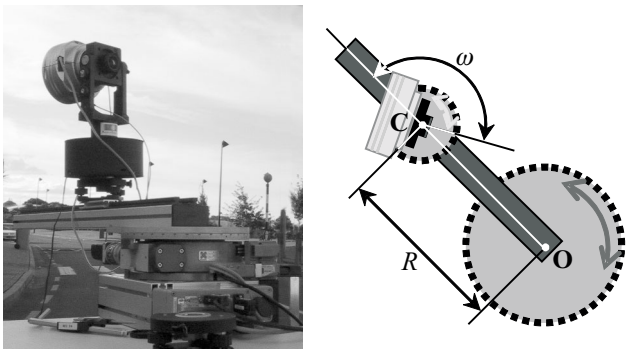

Figure 1: Camera setup for panoramic image acquisition.

The whole equipment is portable and is working with a typical car battery.

2 Calibration

Panoramic cameras are of increasing importance for various applications in computer vision, computer graphics or robotics. Previously developed camera calibration methods (for 'standard' camera architectures following the pinhole camera model) are not applicable due to the non-linearity of the panoramic camera, defined by the existence of multiple (nonlinear) optical centers and a cylindrical image manifold.

First, we discuss a camera calibration method which uses production-site facilities. CCD-line cameras of super-high resolution require extensive geometric and radiometric calibration procedures which concern the 'camera-head'. The main result of the geometric calibration procedure are accurate pixel coordinates in the focal plane in relation to the optical axis (interior orientation). An additional result is a space-dependent point-spread function (PSF), which is related to image resolution and image quality. Ideal parameters (e.g. the focal length f) for characterization of the systems can be derived from this measurements. Radiometric calibration is related to the signal-to-noise-ratio (SNR), signal dynamics and linearity as well as true-color retrieval. Additional measurements concern the homogeneity of the signal, e.g. photo-response non-uniformity (PRNU) and dark-signal non-uniformity (DSNU). All these measurements are done at a special calibration facility (at

*e-mails: {r.klette, g.gimelfarb}@auckland.ac.nz
†e-mail: shoukang@ozawa.ics.keio.ac.jp
‡e-mail: fayhuang@iis.sinica.edu.tw
§e-mails:{Karsten.Scheibe, Martin.Scheele, Anko.Boerner}@dlr.de
¶e-mail: Ralf.Reulke@ifp.uni-stuttgart.de

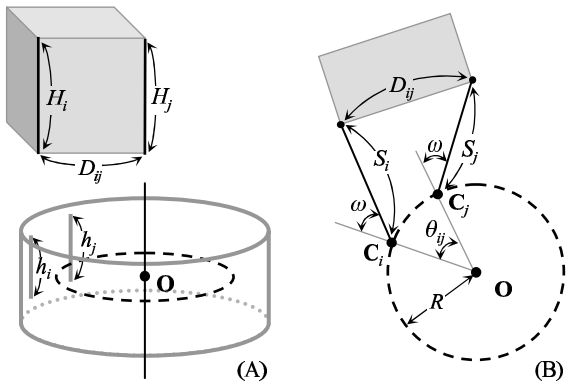

Figure 2: Camera calibration utilizing the parallel line segments in the 3D scene.

DLR Berlin).

Besides these production-site calibrations, the values of the two dominant parameters R and ω have to be dynamically specified according to different scene ranges of interest. The main intention is to find a single linear equation that links 3D geometric scene features to the camera model such that by providing sufficient scene measurements or knowledge (such as distances or lengths) we are able to calibrate accurately the values of R and ω.

We assume that there are at least three straight line segments in the captured real scene (e.g. a special object with straight edges), which are all parallel to the rotation axis. The length of these line segments and the distances[1] between any two parallel lines are measurable.

Consider a pair of parallel line segments of lengths H_i and H_j in 3D space as shown in Fig. 2(A). The distance between these two parallel lines is denoted as D_{ij}. The length of the projections of the line segments on image columns can be determined from the input image, denoted as h_i and h_j in pixels respectively.

Figure 2(B) shows the top view of the geometry. The camera optical centers that see these two parallel lines are denoted as $\mathbf{C}_i$ and $\mathbf{C}_j$ respectively. The distances S_i and S_j are defined to be the shortest distances between the associated camera optical centers and the parallel lines respectively, and can be calculated by the following relations

$$S_i = \frac{f H_i}{h_i} \text{ and } S_j = \frac{f H_j}{h_j},$$

where f is the pre-calibrated effective focal length of the (line-) camera. The angular distance θ_{ij} ($\angle\, \mathbf{C}_i\mathbf{O}\mathbf{C}_j$) can be calculated as follows:

$$\theta_{ij} = \frac{2\pi d_{ij}}{W},$$

where d_{ij} is the distance between two projections of the parallel lines on image, measured in pixel, and W is the width of a panorama in pixels.

We obtain a linear equation as follows:

$$\begin{aligned} 0 &= (1-\cos\theta_{ij})R^2 \\ &+ (S_i+S_j)(1-\cos\theta_{ij})R\cos\omega \\ &- (S_i-S_j)\sin\theta_{ij}R\sin\omega \\ &+ \frac{S_i^2+S_j^2-D_{ij}^2}{2} - S_iS_j\cos\theta_{ij}. \end{aligned} \quad (1)$$

[1]The distance between two parallel lines is the length of a line segment that connects both lines and which is perpendicular to these lines.

Since the values of S_i, S_j, D_{ij}, and θ_{ij} are known, the equation can be arranged into the following form,

$$K_1X_1 + K_2X_2 + K_3X_3 + K_4 = 0,$$

where $K_i, i = 1, 2, 3, 4$, are coefficients. The three linearly independent variables are

$$\begin{aligned} X_1 &= R^2 \\ X_2 &= R\cos\omega \quad \text{and} \\ X_3 &= R\sin\omega. \end{aligned}$$

Because of the dependency among the variables X_1, X_2, and X_3, there are multiple solutions of R and ω, if we solve it by a linear least-square technique. To tackle this multiple-solutions problem, we may constrain the parameter estimation further by the inter-relation among X_1, X_2, and X_3, which is

$$X_1^2 = X_2^2 + X_3^2$$

because of

$$R^2 = (R\cos\omega)^2 + (R\sin\omega)^2.$$

Assume that n equations are given. We want to minimize the following:

$$min \sum_{i=1}^{n} \left(K_{1n}X_1 + K_{2n}X_2 + K_{3n}X_3 + K_{4n}\right)^2, \quad (2)$$

subject to the equality constraint $X_1 = X_2^2 + X_3^2$, where the values of $K_{in}, i = 1, 2, 3, 4$, are calculated based on the measurements from real scenes and the image, and $X_1 = R^2$, $X_2 = R\cos\omega$, and $X_3 = R\sin\omega$. Now, the values of R and ω can be found uniquely by

$$R = \sqrt{X_1}$$

and

$$\omega = \arccos\left(\frac{X_2}{\sqrt{X_1}}\right).$$

Note that even though the additional constraint forces that a non-linear optimization method to be used, the expected linear parameter estimation quality remains.

3 Stereo Visualization

We discuss two possible applications of symmetric panoramic images $E_{\mathcal{P}_R}(R,\, f,\, \omega,\, \gamma)$ and $E_{\mathcal{P}_L}(R,\, f,\, (2\pi-\omega),\, \gamma)$. A pair of symmetric panoramic images is captured during one rotation of the panoramic camera. We start with stereo visualization in this section.

3.1 Spatial Sampling

Spatial sampling describes how a 3D space is sampled without considering underlining structures or the complexity of 3D scenes. Studies of spatial sampling for image acquisition are of great importance for vision applications.

A spatial sample is defined by intersections of projection rays. Figure 3 illustrates top views of spatial sample formations of a stereo panoramic pair in the outward case[2]. The camera model is depicted in Fig. 3(A). Projection rays emitting panoramically from projection centers on the base circles, are shown in Fig. 3 (B) and

[2]The associated principal angle ω is less than or equal to $\frac{\pi}{2}$ or is greater than or equal to $\frac{3\pi}{2}$.

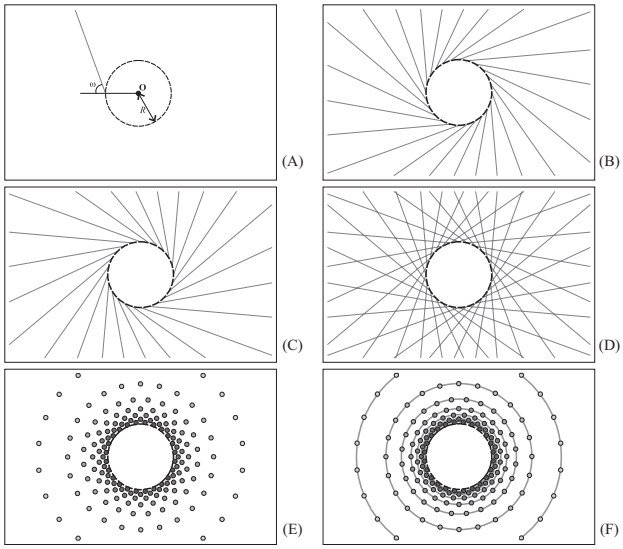

Figure 3: Sampling structure in the outward case.

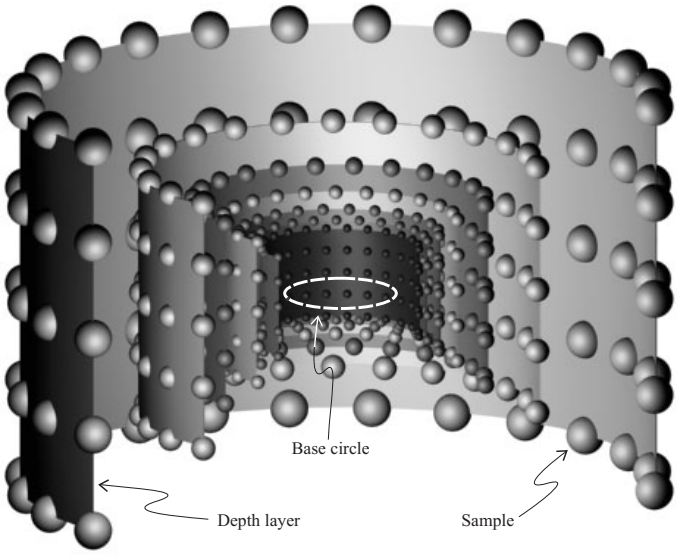

Figure 4: A 3D view of sampling structure in outward case.

(C) for the right and left stereo panoramas, respectively. Superimposing Fig. 3 (B) and (C), we have Fig. 3 (D) which reveals the basic structure of stereo samples, that is, the concentric circles formed by the intersections of the projection rays.

Figure 3 (E) removes the projection rays in Fig. 3 (D), and replaces the intersections by small colored circles (the darker the closer to **O**). In Fig. 3 (F), the sampling structure are augmented with supporting concentric circles in gray. Note that the innermost dashed black circle is the base circle; one should not confuse it with the supporting concentric circles. Radiuses of the concentric circles increase non-linearly. The 'concentric circles' are indeed concentric cylinders in 3D. Motivated by the fact that samples are layered in depth (the distance from **O**), we refer to these concentric circles (cylinders in 3D) as *depth layers*.

The 3D visualization of a sampling structure corresponding to Fig. 3 (F) is depicted in Fig. 4. The samples are drawn at different sizes (i.e. larger as they are further away from **O**) and at different colors for different depth layers. Only samples of 240° views are shown for clearness. The structure of depth layers can be described by a set of equal-height concentric cylinders whose tops and bottoms are cut-off by a pair of co-axis hyperboloid symmetric to the base plane[3]. The observation can also be confirmed by the fact that the epipolar surface for stereo panoramas is a half-hyperboloid [Seitz 2001]. This observation helps in further modeling for studying geometric relations of scenes, application constraints and acquisition systems.

Since the diversity of sample densities and density distributions is influenced by the range of ω and possible R values, it is not difficult to infer the advantageous flexibility of the acquisition model permitting an advanced control of spatial sampling over a dynamic range of scenes. This consequence motivates us further to study these two camera parameters, especially for image quality control and the camera analysis and design problems, which will be discussed in the later subsection. Sampling resolution is defined as the total number of samples in 3D space. It gives a measure of sampling density and characterizes spatial sampling in a general sense. We have the following theorem.

Theorem 3.1 *Given a pair of stereo panoramas of image resolution $W \times H$, and the value of the associated principal angle of both images is ω, where $\omega \in (0^\circ, 180^\circ)$. The total number of spatial samples, namely spatial sampling resolution of the stereo panoramas, is equal to*

$$W \times H \times \left\lfloor \frac{\omega W}{180^\circ} \right\rfloor . \tag{3}$$

Consider a pair of stereo panoramas, when the value of the associated principal angle ω equals to 0° or 180°, there is no sample. The value of the off-axis distance R of a stereo panorama pair has no impact onto the spatial sampling resolution. The spatial sampling resolution of a stereo panoramic pair increases as the value of the associated ω increases in the range $(0^\circ, 180^\circ)$. In the outward case, i.e. $0^\circ < \omega \leq 90^\circ$, the spatial sampling resolution of a stereo panoramic pair reaches its maximum for an associated principal angle $\omega = 90^\circ$, and this result coincides with a result reported in [Shum et al. 1999].

3.2 Quality Control

We denote by *image quality control* a method which ensures proper configurations of camera settings such that image quality meets the requirements or criteria defined by an application under the assumption that a capable and accurate camera system is used. The development of such an image quality control method requires a basic understanding of geometric and/or photometric relations among the camera system, 3D scene complexities, and application requirements.

In this paper, two main quality control problems of stereo panorama imaging are discussed: *scene composition* and *stereo acuity*. The scene composition problem is "how the camera's parameter values should be set such that the intended scenes or subjects are composed desirably in the resultant images?", without involving any subjective issues of scene composition. Without a proper control of scene composition, the resultant images may miss important features, might be inexpressive for the subjects, or may possibly cause ambiguities or incoherence.

The stereo acuity control is to analyze how the camera parameters can be set such that the resultant number of depth layers meet the stereo acuity requirement in an application, for a specified family of scenes of interest. Insufficient stereo acuity over the relevant

[3]The plane where the base circle lies on.

	D_1	D_2	H_1	W	θ_w	R	ω
(1)	1	3	1.2	16232	10.48	0.2499	146.88
(2)	4	10	4.2	18550	9.17	0.5809	113.92
(3)	6	50	5.5	21249	8.00	0.6768	44.66
(4a)	20	200	20.0	19478	8.74	1.6942	92.43
(4b)	20	200	20.0	19478	5.00	0.9695	91.39
H = 5184 (pixels) H_S = 768 (pixels)				u = 0.007 (mm) f = 21.7 (mm)			

Table 1: The results of the determined control values of R and ω and the given conditions in four typical examples.

interval of distance values for a given 3D scene of interest produces a *cardboard effect* [Yamanoue et al. 2000], i.e. the 3D scene is perceived as a set of 'parallel cardboards', sorted in depth, one sitting in front of the next one. On the other hand, stereo acuity greater than the upper disparity limit of human vision causes double images, called *dipopia*, which results in uncomfortable stereoscopic viewing as well as eyestrain [Viire 1997; Siegel et al. 1999; Ijsselsteijn et al. 2000; Mayer et al. 2000].

Four parameters are introduced. The first two parameters describe the range of scenes of interest by D_1 and D_2 as nearest and furthest distances from **O** where the quality control is applied to. And the third parameter H_1 is defined by the distance between an optical center **C** and a point on the base plane in distance D_1 from **O**; we call it *distance to target range*. The last parameter θ_w is the width of the angular disparity interval for the nearest and furthest 3D points in the range of scenes of interest with respect to **O**.

Now we assume that values of these four parameters D_1, D_2, H_1, and θ_w are specified with respect to the intended scenes and the application particulars. What values of camera parameters, i.e. off-axis distance R and principal angle ω, should be chosen such that the demanded quality of scene composition and the stereo acuity can be realized? We answer this question in the following theorem.

Theorem 3.2 *While the parameters D_1, D_2, H_1, and θ_w are bounded, there exists a unique solution for both off-axis distance R and principal ω satisfying the geometric constraints of scene composition and stereo acuity for a stereoscopic panoramic camera:*

$$R = \sqrt{D_1^2+H_1^2+2D_1H_1\frac{D_1-D_2\cos\left(\frac{\theta_w}{2}\right)}{\sqrt{D_1^2+D_2^2-2D_1D_2\cos\left(\frac{\theta_w}{2}\right)}}}$$

and

$$\omega = \arccos\left(\frac{D_1D_2\cos\left(\frac{\theta_w}{2}\right)-D_1^2-H_1\sqrt{A}}{\sqrt{A(D_1^2+H_1^2)+2D_1H_1(D_1-D_2+\cos\left(\frac{\theta_w}{2}\right))\sqrt{A}}}\right),$$

where $A = (D_1^2 + D_2^2 - 2D_1D_2\cos\left(\frac{\theta_w}{2}\right))$.

Since the solution for the camera parameters is unique, neither the camera parameter R nor ω can adequately satisfy the stereoscopic panorama quality requirement alone. Using the computed control values, the image quality of stereoscopic panoramas with respect to scene composition and stereo acuity criteria can be ensured at acquisition time. As only three on-site measures are required (i.e. D_1, D_2, H_1) the overheads in addition to the original imaging process are acceptable.

Four examples of commonly occurring situations are given to demonstrate the results of the control values of R and ω. The examples, shown in Tab. 1, include (1) a close-range indoor scene covering an area of about $9m^2$; (2) a far-range indoor scene of an area of about $100m^2$; (3) an outdoor or open-area scene with a closer RoI between 6 to 50 meters away from the center; and (4) an outdoor scene with a further RoI of about 20 to 200 meters from the center.

The supporting parameters include the effective focal length $f = 21.7mm$, pixel size $u = 0.007mm$, panoramic image height $H = 5184$ in pixels, and the display screen height $H_S = 768$ in pixels. The parameters D_1, D_2, H_1 and R are measured in meters, θ_w and ω in degrees, and W in pixels. To allow that acquired stereoscopic panoramas are directly fusible and that viewing is comfortable at a specific display screen resolution, we have

$$\theta_w = \frac{2\pi d_w H}{W H_S},$$

where $d_w = 70$ pixels are used in all four cases for a 17" display screen (1024x768 pixels) viewing at $40cm$ frontal position over both crossed and uncrossed disparity fields. Note that the term $\frac{H}{H_S}$ allows that the acquired full vertical perspective is rendered on the full screen. To allow interactive zooming in stereoscopic visualization, the stereo-shifts must be dynamically adapted such that the desired quality of 3D perception is ensured.

The results of the determined control values of R and ω in Tab. 1 show the actual values satisfying the scene composition and stereo acuity requirements under the given conditions. The values of principal value ω in the first two examples illustrate the capability of a stereoscopic panoramic camera in adaptation to close-range condition, that is, ω 90°. Such an adaptability reveals an advantage of using a stereoscopic panoramic camera over the traditional single-center panoramic camera. The values of R computed in examples (1-3) are actually realizable using the setup as shown in Fig. 1 because the extension slider can support the value of R up to $1m$. In the example (4a), however, we have an hardware-unachievable case where the determined value of R is over $1m$. To illustrate the trade-off for a possible values of $R < 1m$, we have reduced the stereo acuity θ_w to 5° in the example (4b).

4 Stereo Image Analysis

The second application of symmetric panoramic images is depth or shape recovery.

4.1 Epipolar Geometry

The study of epipolar geometry is essential for the applications such as 3D reconstruction from panoramic images, visualization or simulation of walk-through, i.e. the virtual paths created between multiple panoramas. The epipolar curve equation serves as a fundamental tool for many important computer vision tasks, such as pose estimation and stereo analysis.

The general epipolar curve equation for a pair of arbitrary polycentric panoramas is presented by the following theorem.

Theorem 4.1 *Let (x_1, y_1) and (x_2, y_2) denote the image coordinates of the projection of a 3D point in the source image $E_{\mathcal{P}_1}$ and the destination image $E_{\mathcal{P}_2}$, respectively. Consider x_1 and y_1 as being given. Let $\alpha_1 = \frac{2\pi x_1}{\mu W_1}$, $\alpha_2 = \frac{2\pi x_2}{\mu W_2}$, $\delta_1 = (\alpha_1 + \omega_1)$, $\delta_2 = (\alpha_2 + \omega_2)$, and $\beta_1 = \arctan(\frac{y_1}{f_1})$. The corresponding epipolar curve on the destination image $E_{\mathcal{P}_2}$ cab be represented by the equation*

$$y_2 = \frac{f_2\boldsymbol{r}_2^T\cdot\boldsymbol{V}}{\sin\delta_2\boldsymbol{r}_1^T\cdot\boldsymbol{V} + cos\delta_2\boldsymbol{r}_3^T\cdot\boldsymbol{V} - R_2\cos\omega_2},$$

which is only valid if the value of the denominator is greater than zero. The vector $\boldsymbol{V}$ is defined as follows:

$$\boldsymbol{V} = \boldsymbol{A} + \frac{R_2\sin\omega_2 + \cos\delta_2\boldsymbol{r}_1^T\cdot\boldsymbol{A} - \sin\delta_2\boldsymbol{r}_3^T\cdot\boldsymbol{A}}{\sin\delta_2\boldsymbol{r}_3^T\cdot\boldsymbol{B} - \cos\delta_2\boldsymbol{r}_1^T\cdot\boldsymbol{B}}\boldsymbol{B},$$

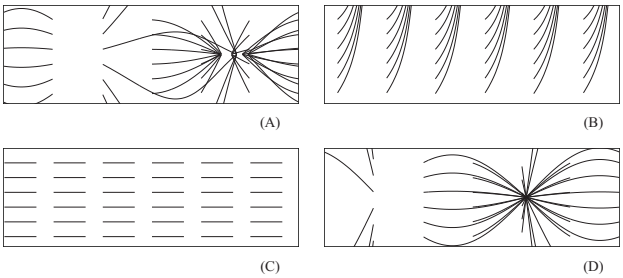

Figure 5: Epipolar curves of four special cases: (A) leveled; (B) concentric; (C) symmetric; and (D) single-center panoramas.

where

$$\boldsymbol{A} = \begin{pmatrix} R_1 \sin\alpha_1 - t_x \\ -t_y \\ R_1 \cos\alpha_1 - t_z \end{pmatrix} \text{ and } \boldsymbol{B} = \begin{pmatrix} \sin\delta_1 \cos\beta_1 \\ \sin\beta_1 \\ \cos\delta_1 \cos\beta_1 \end{pmatrix}.$$

Furthermore, the matrix $[\boldsymbol{r}_1^T \boldsymbol{r}_2^T \boldsymbol{r}_3^T]^T$ *and the vector* $(t_x, t_y, t_z)^T$ *specify the orientation and the position of the panoramic camera of* $E_{\mathcal{P}_2}$ *with respect to the camera coordinate system of the panoramic camera of* $E_{\mathcal{P}_1}$.

An intuitive and practical way to reduce the dimensionality of the general epipolar curve equation is to make all the associated axes of the panoramas leveled to the sea level. It can be achieved by mounting the camera on a leveled tripod. A polycentric panoramic pair whose associated axes are orthogonal to the sea level is called *leveled panoramic pair*.

Note that the heights of images in a leveled panoramic pair can be different. Under the assumption that a panoramic pair is perfectly leveled, the general epipolar curve equation in Theorem 4.1 can be simplified. We have the following corollary.

Corollary 4.2 *Let* (x_1, y_1) *and* (x_2, y_2) *be a pair of corresponding image points in a pair of leveled polycentric panoramas* $E_{\mathcal{P}_1}(R_1, f_1, \omega_1, \gamma)$ *and* $E_{\mathcal{P}_2}(R_2, f_2, \omega_2, \gamma)$*, respectively. Given* x_1 *and* y_1*, the epipolar curve equation in this case can be simplified as follows:*

$$y_2 = \frac{y_1 \left(\frac{f_2}{f_1}\right)(\boldsymbol{K}) - t_y f_2 \sin(\sigma_2 - \sigma_1)}{R_2 \sin(\sigma_1 - \alpha_2 - \phi) - R_1 \sin\omega_1 - t_x \cos\sigma_1 + t_z \sin\sigma_1},$$

where $\alpha_1 = \frac{2\pi x_1}{\mu W_1}$, $\alpha_2 = \frac{2\pi x_2}{\mu W_2}$, $\sigma_1 = (\alpha_1 + \omega_1)$, $\sigma_2 = (\alpha_2 + \omega_2 + \phi)$*, the angle* ϕ *determines the rotation with respect to the y-axis, and* $\boldsymbol{K} = R_2 \sin\omega_2 - R_1 \sin(\sigma_2 - \alpha_1) - t_x \cos\sigma_2 + t_z \sin\sigma_2$.

Two panoramas whose axes coincide are called a *co-axis panoramic pair*. This constraint reduces two rotational and two translational parameters, and yet has its practical merit. The epipolar curves of a co-axis pair coincide with image columns under some camera setting assumptions. Also note that the implementation of such a configuration is reasonably straightforward. A normal tripod allows such a setting. Therefore, this geometrical constraint has been commonly applied in some panoramic camera architectures such as the catadioptric approach [Southwell et al. 1996; Gluckman et al. 1998; Nene and Nayar 1998; Petty et al. 1998].

The epipolar geometry of a co-axis panoramic pair is characterized in the following corollary.

Figure 6: Stereo pair of panoramic images brought to the standard epipolar geometry by rectifying the epipolar curves.

Corollary 4.3 *Let* (x_1, y_1) *and* (x_2, y_2) *be a pair of corresponding image points in a co-axis pair of panoramas. Given* x_1 *and* y_1*, we have*

$$y_2 = \frac{y_1 \left(\frac{f_2}{f_1}\right)(R_2 \sin\omega_2 - R_1 \sin(\sigma_2 - \alpha_1)) - t_y f_2 \sin(\sigma_2 - \sigma_1)}{R_2 \sin(\sigma_1 - \alpha_2 - \phi) - R_1 \sin\omega_1},$$

where $\alpha_1 = \frac{2\pi x_1}{\mu W_1}$, $\alpha_2 = \frac{2\pi x_2}{\mu W_2}$, $\sigma_1 = (\alpha_1 + \omega_1)$ *and* $\sigma_2 = (\alpha_2 + \omega_2 + \phi)$*, and the angle* ϕ *determines the rotation with respect to the y-axis.*

Figure 5 illustrates the distinctiveness of epipolar curve patterns in four different geometric configurations: leveled; concentric; symmetric; and single-center panoramas.

4.2 Stereo Matching

Due to the known epipolar curves, the panoramic pair can easily be converted into the standard horizontal epipolar stereo pair having one-to-one correspondence between the pixel rows in the both images. Assuming a continuous visible surface, binocular stereo reconstruction of the panoramic scene can be obtained by one or another conventional stereo technique, e.g., by symmetric dynamic programming stereo (SDPS) [Gimel'farb 2002].

Figures 6 and 7 show the left and right stereo images of a close-range urban 3D scene and results of 3D stereo reconstruction with the SDPS (namely, the range image with the grey-coded depths and the ortho image fusing the stereo images in accord with visibility of the reconstructed 3D points).

Some reconstruction errors, e.g. on the sky or near the right-most columns of the building are typical for these panoramic line cameras. Because of relatively long time for capturing a single image, the left and right images of the stereo pair differ considerably in all the "dynamically changing" areas such as cloud patterns or positions of moving people.

5 Multi-Sensor-Approach

The combination of geometric 3D laser scanner data and high resolution panoramic color image data opens up new possibilities

Figure 7: Range and ortho images of the reconstructed 3D scene.

in architectural documentation and digitalization; in particular for preservation of historic buildings and monuments. Distance measurements of a laser scanner provide high-resolution digital surface models. Due to extremely high resolution, panoramic images are suitable for "texture mapping" in rendering of such high-resolution surface models. Figure 5 illustrates one panoramic scan, which can be used for high quality texture mapping. Data acquisition is based on a panorama scanner for color images and a laser scanner for 3D information [Scheibe et al. 2001].

The data sets (range data and panoramic images) are co-registered to reference each other and transformed into theodolite measurements using photogrammetric bundle adjustment. Measured or calculated orientation data can be used to merge 3D scanner pixels and 2D color pixels in a virtual information space in order to generate different views, ortho images or 3D models.

The combination of laser scanner data with digital scanner panoramas is very useful in close range photogrammetry. As an example, results of the "Neuschwanstein project" are presented. The project is directed on a complete 3D photometric documentation of this Bavarian castle.

Figure 8: Panoramic scan of the castle Neuschwanstein.

The range and image data are transformed into a theodolitic (spherical) coordinate system with two angles, longitude σ and latitude τ, and one distance value ρ for each pixel. In both systems we have along the rotation axis data in fixed angle increments, dependent from the cylindrical recording system. The vertical angle (latitude) results from the equations:

$$\tau = arctan(i \cdot d/f)$$

with the number i of vertical pixels with pixel size d and the focal length f of the camera. The distance to the object is unknown. The strategy to capture the distance data with the 3D laser scanner is similar to that of close range photogrammetry. A conventional gray scale image in addition to the 3D data enables immediate control of the recorded data. Figure 5 shows a laser scanner reflection image from the scene shown in Fig. 5.

Figure 9: Intensity image of a laser scan.

The laser scanner data are already in a theodolitic coordinate system. The first step is to convert the scanner data into a format where the distance and the intensity data are stored in a 3D grid with equidistant angle increments. This reduces the size of the data by about a third. Calibration information is crucial for this reduction step.

The advantage of laser scanner data is the possibility to view the data after a scan immediately in 3D space (with rotation, translation or scaling).

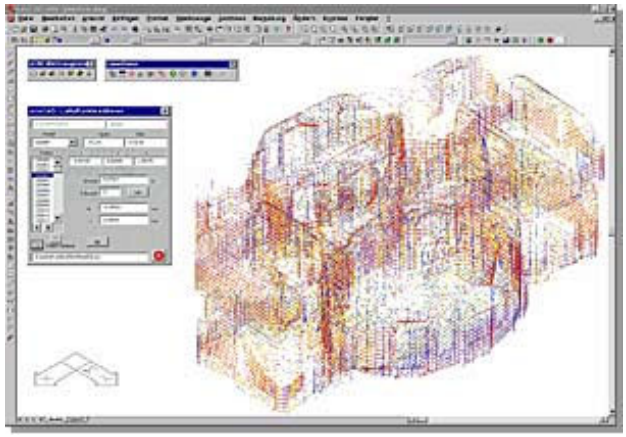

Figure 10: 3D view of laser scanner data.

Laser scanner and camera work digitally, and the accuracy of the whole 3D digitalization and modeling approach critically depends on calibration of the systems: calibration of the rotation table of the panorama camera, and of the off-axis distance between rotation axis and projection center of the optics [Huang 2002]. The viewing angle ω was kept at zero degree.

A single scan is in general not sufficient to acquire all object points due to visibility limitations. Several panorama scans from different view points require 3D modelling such that texture mapping can be based on object matching. This is done automatically by identifying control points and other characteristic points or patterns, followed by bundle adjustment. The results are seven parameters of an affine transform including scaling (3 translation, 3 rotation, and one scaling parameter) of the exterior orientation of every scan. The same method is used to orientate the panoramic image data to the laser scan data. In addition it is possible to improve the parameters of the scanners interior orientation. If an oriented virtual 3D model is given consisting of any number of scans, any desired layout maps, elevations, scene views, or 3D object visualizations can be created.

The next step is to map panoramic image data (“texture”) on the laser scan based CAD model. The difficulty arises from the amount of data: one scan has more than 270 million pixels, and often there are more than just one panoramic image for one scene. Normal ray tracing algorithms require extensive computations.

Alternatively, we generated 3D surface models based on dynamically generated (optimized) triangular meshes [Gimel’farb et al. 1972]. Parameters can be set to provide the required degree of detail. The size of the meshes depends on the structure of the surface. Planar surface patches generate ‘rough’ meshes, and fine structures have detailed meshes.

The following figure illustrated the result of panoramic image mapping for a detail of Neuschwanstein, where the surface is approximately planar. First an ortho plane was defined, and the orientated panorama data are projected onto this plane.

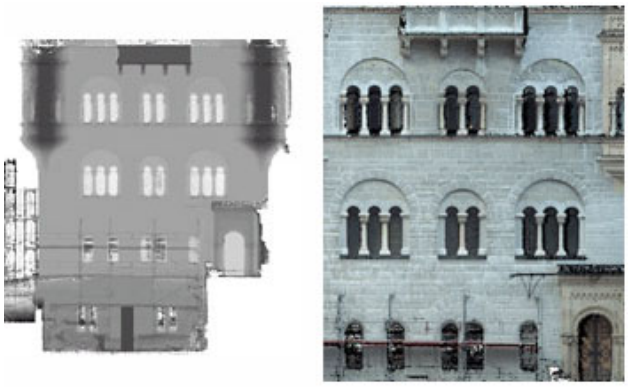

Figure 11: Left: gray coded surface, right: with mapped texture.

Ortho images are generated by merging 3D object surfaces and photographic information. High resolution photos need to be taken into account in addition to the laser scans. Figure 5 shows a detail of the original panorama data and the result after texture mapping onto the laser surface data.

Figure 12: Left: original panorama image, right: processed ortho image.

In some cases the acquisition of 3D data from a stereo analysis module was replaced by a combination of laser data and color panoramic images. However, computation time saved by using laser data instead of stereo processing, is then needed for rendering and raytracing. It also required the development of a fast algorithm, which handles more than 1500 million points and takes advantage of the reported research on rotations and epipolar geometry of panoramic images. Mesh calculations for visualizing very large clouds of 3D points is not yet solved acceptable. Figure 5 shows a visualization of a 3D scene on a regular raster.

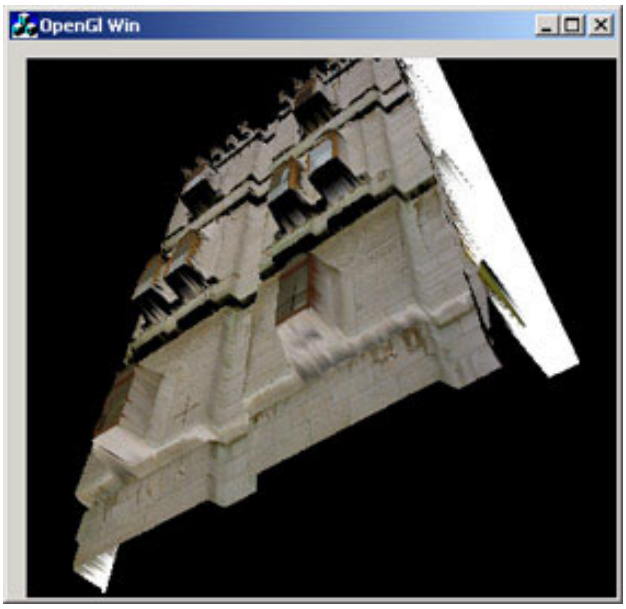

Figure 13: OpenGl application for viewing a 3D result.

6 Conclusion

We reviewed recent developments in fundamental research, production and application of cylindrical panoramic cameras. Major ‘milestones’ have been set, but future research and design has to address more specific questions. For example, the impact of inaccurate rotations on epipolar geometry is one of these subjects, and the unification of several 3D distance maps produced by several stereo pairs of symmetric panoramic images is another (difficult) subject.

The acquisition of 3D laser scan data can be accompanied by stereo panoramic images in order to improve the quality of the surface model derived from the laser scanner. Problems resulting from reflections on edges and corners might be solvable this way. Stereo processing of panoramic images has already started as shown in this article.

References

GIMEL’FARB, G., MARCHENKO, V., AND RYBAK, V. 1972. An algorithm for automatic identification of identical sections on stereo pairs of photographs. *Cybernetics 8*, 2, 311–322.

GIMEL’FARB, G. 2002. Probabilistic regularisation and symmetry in binocular dynamic programming stereo. *PRL 23*, 4 (February), 431–442.

GLUCKMAN, J., NAYAR, S., AND THOREK, K. 1998. Real-time panoramic stereo. In *Proc. DARPA’98*, 299–303.

HUANG, F. 2002. *Epipolar Geometry and Camera Calibration of Cylindrical Panoramas*. PhD thesis, CITR, Computer Science Department, The University of Auckland, Auckland, New Zealand.

IJSSELSTEIJN, W. A., DE RIDDER, H., AND VLIEGEN, J. 2000. Effects of stereoscopic filming parameters and display duration on the subjective assessment of eye strai. In *Proc. SDVRS VII*, 12–22.

KLETTE, R., GIMEL'FARB, G., AND REULKE, R. 2001. Wide-angle image acquisition, analysis and visualization. In *Proc. 14th Internat. Conf. "Vision Interface" (VI'2001)*, 114–125.

MAYER, U., NEUMANN, M., KUBBAT, W., AND LANDAU, K. 2000. Is eye damage caused by stereoscopic displays? In *Proc. SDVRS VII*, 4–11.

NENE, S., AND NAYAR, S. 1998. Stereo with mirrors. In *ICCV98*, 1087–1094.

PETTY, R., ROBINSON, M., AND EVANS, J. 1998. 3d measurement using rotating line-scan sensors. *Measurement Science and Technology 9*, 3, 339–346.

SCHEIBE, K., KORSITZKY, H., AND REULKE, R. 2001. Eyescan - a high resolution digital panoramic camera. In *Proc. Robot Vision 2001*, 77–83.

SEITZ, S. 2001. The space of all stereo images. In *Proc. ICCV'01*, 26–33.

SHUM, H., KALAI, A., AND SEITZ, S. 1999. Omnivergent stereo. In *Proc. ICCV'99*, 22–29.

SIEGEL, M., TOBINAGA, Y., AND AKIYA, T. 1999. Kinder gentler stereo. In *SPIE Proc. Stereoscopic Displays and Applications X*, 18–27.

SOUTHWELL, D., REYDA, J., FIALA, M., AND BASU, A. 1996. Panoramic stereo. In *ICPR'96*, A:378–382.

VIIRE, E. 1997. Health and safety issues for vr. *Communications of the ACM 40*, 8, 40–41.

WEI, S.-K. 2002. *Analysis, Design, and Control of Stereoscopic Panoramic Imaging*. PhD thesis, CITR, Computer Science Department, The University of Auckland, Auckland, New Zealand.

YAMANOUE, H., OKUI, M., AND YUYAMA, I. 2000. A study on the relationship between shooting conditions and cardboard effect of stereoscopic images. *IEEE Tran. on Circuits and Systems for Video Technology 10*, 3, 411–416.